

the nonlinear evolution of a kinetic magnetosonic wave (19).

We conclude that there is presently no clearly dominant mechanism that makes Deimos such an effective obstacle to the solar wind, although the idea of a charged ion cloud around Deimos is favored. Future international space missions to Mars (Mars-96, Mars-Observer, Planet-B) will certainly improve our knowledge about the plasma-dust environment of the martian moons. Three-dimensional simulations of the dynamical response of a magnetoplasma to small celestial bodies are also necessary. This modeling could be used as a tool for remote sensing of physical properties of the martian moons and asteroids.

REFERENCES AND NOTES

1. K. Baumgärtel and K. Sauer, *Ann. Geophysicae* **10**, 763 (1992); K. Sauer *et al.*, *Geophys. Res. Lett.* **20**, 165 (1993); U. Motschmann *et al.*, *ibid.*, **19**, 225 (1992); K. Baumgärtel and K. Sauer, *Adv. Space Res.* **13**, 291 (1993).
2. W.-H. Ip and K. Banaszekiewicz, *Geophys. Res. Lett.* **17**, 857 (1990).
3. E. M. Dubinin *et al.*, *ibid.*, p. 861.
4. A. V. Bogdanov, *J. Geophys. Res.* **86**, 6926 (1981).
5. E. M. Dubinin *et al.*, *Planet. Space Sci.* **39**, 123 (1991).
6. F. Herbert, *Adv. Space Res.* **13**, 249 (1993).
7. K. Sauer *et al.*, *Geophys. Res. Lett.* **21**, 2255 (1994).
8. D. L. Book *et al.*, in *Finite-Difference Techniques for Vectorized Fluid Dynamics Calculations*, D. L. Book, Ed. (Springer, New York, 1981), p. 29.
9. F. P. Fanale and J. R. Salvail, *Geophys. Res. Lett.* **16**, 287 (1989).
10. M. Horanyi *et al.*, *ibid.* **17**, 853 (1990); A. Juhasz *et al.*, *J. Geophys. Res.* **98**, 1205 (1993); H. Ishimoto and T. Mukai, *Planet. Space Sci.* **42**, 691 (1994).
11. E. Dubinin, *Adv. Space Res.* **13**, 10271 (1993).
12. M. Kivelson *et al.*, *Science* **261**, 331 (1993).
13. M. Kivelson *et al.*, *Adv. Space Res.* **16**, 459 (1995).
14. K. Baumgärtel, K. Sauer, A. Bogdanov, *Science* **263**, 653 (1994).
15. C. K. Goertz, *Planet. Space Sci.* **32**, 1387 (1984); R. Stenzel, J. Urrutia, C. Rousculp, *Phys. Fluids B* **5**, 325 (1993).
16. M. Terho *et al.*, in *Abstracts for "Small Bodies in the Solar System and their Interaction with the Planets,"* H. Rickman and M. Dahlgren, Eds. (Mariehamn, Åland, Finland, 1994), p. 159.
17. L. J. Smka, in *Proton and Particle Interactions with Surfaces in Space*, R. J. Grard, Ed. (Reidel, Boston, 1973), p. 481; A. Barnett and S. Olbert, *J. Geophys. Res.* **91**, 10117 (1986).
18. W.-H. Ip and F. Herbert, *Moon Planets* **28**, 43 (1983).
19. N. Omidi and D. Winske, *J. Geophys. Res.* **95**, 2281 (1990).
20. We are grateful to the FGMM team, and also K. Schwingenschuh and R. Grard for providing of magnetometers and the probe data. The work was done while E.D. visited Max-Planck-Institut für extraterrestrische Physik, which he thanks for their financial support and hospitality in Berlin.

6 March 1995; accepted 6 July 1995

Photodeposition of Micrometer-Scale Polymer Patterns on Optical Imaging Fibers

Brian G. Healey, Stacy E. Foran, David R. Walt*

Microstructures were fabricated on optical imaging fibers with a photopolymerization technique. Monodisperse polymeric microarrays were produced containing spots of 2.5 micrometers in diameter spaced 4.5 micrometers apart. Polymer microarrays were also deposited on other substrates by using imaging fibers for light delivery. The technique allows micrometer-scale photopatterning with masks larger than the desired dimensions.

There has been considerable interest in preparing micrometer- and nanometer-scale structures such as nanotubes (1), nanowires (2), quantum dots (3), microspheres (4), and nanometer-size light-emitting diodes (5). Complex, well-defined microstructures have been produced by techniques including laser-assisted chemical vapor deposition (6) and the creation of hydrophobic templates from photoresists for the deposition of self-assembled monolayers on gold (7). Photoactivation techniques have also been used to fabricate well-defined microstructures; for example, photolithography has been used for information storage in photoconductive materials (8), photoassembly of combinatorial

libraries (9), and site-selective covalent attachment of biomolecules (10). Here we report a simple technique for the fabrication of patterned microstructures. Specifically, we use the discrete light pathways in an optical imaging fiber to photopolymerize an array of individual polymer spots in a variety of sizes and patterns.

Optical imaging fibers are hexagonally packed bundles of individual fibers melted and drawn together so as to maintain the same relative position for each fiber in the bundle throughout its length (11). Such bundles can carry coherent images from one end of the bundle to the other and have been used extensively for medical imaging. The present technique is based on chemistry developed in our laboratory for preparing fiber-optic sensors (12). The distal end of an imaging fiber is first functionalized by treatment with 3-trimethoxysilylpropylmethac-

rylate to attach a photopolymerizable acrylate group to the glass surface which facilitates the adhesion of the polymer to the glass surface. The fiber is then placed on the photodeposition system (Fig. 1A). Collimated light from a mercury-xenon arc lamp is passed through a neutral density filter slide and then through an excitation bandpass filter to isolate the appropriate initiation light. The initiation light passes through a mask and is imaged onto the proximal end of the fiber (Fig. 1B). The distal end of the fiber is then coated with a thin film of prepolymer by dipping it in a small volume of solution containing photoinitiator, solvent, and a monomer or oligomer that can be photocrosslinked (13). The fiber is then illuminated for a fixed time by an electronic shutter (14), and the excess polymerization solution is removed by rinsing with ethanol.

First we produced microstructures by using a pinhole mask and placing a focusing lens between the excitation filter and the pinhole (Fig. 2, A and B). A 25- μm -diameter spot was imaged onto the fiber. Polymer formed only on the individual fiber cores because the glass claddings between the fibers of the bundle do not propagate light. In Fig. 2A, the hexagonal packing of the 2- to 3- μm -diameter polymer spots is seen clearly with a spacing between spots (center to center) of 4 to 5 μm . This pattern corresponds identically to the individual pixels of the imaging fiber. The side view of the pattern shows that the polymer spots are approximately 2 to 3 μm in height and appear as hemispheres on the fiber surface (Fig. 2B). The polydispersity of the polymer microspots is due to the gaussian distribution of light exiting the pinhole and the type of imaging fiber used. Polymer spots on the edges are smaller as a result of decreased light intensity, and the noncircular polymer spots (Fig. 2A, top view) are a result of nonuniform fibers in the bundle. Monodisperse polymeric microstructures were fabricated with a defect-free imaging fiber (Fig. 2C) and had polymer spots 2.5 μm in diameter, spaced 4.5 μm apart, and 1.2 μm high (15).

On careful examination of a scanning electron micrograph (SEM) from a different polymer array preparation, we observed that triangular wells with 1- μm edges could be produced by controlling the polymerization reaction composition and time carefully (Fig. 2D). The wells were fabricated by increasing the concentration of photocrosslinkable oligomer and increasing the illumination time. During polymerization, the polymer first deposits on the fiber cores and then continues to deposit between the fibers where the cores have their closest approach. The polymer wall between the wells is less than 0.5 μm wide and 1.0 μm high. The triangular wells have a volume of 460 al (1 al

Max Tishler Laboratory for Organic Chemistry, Department of Chemistry, Tufts University, Medford, MA 02155, USA.

*To whom correspondence should be addressed.

Fig. 1. (A) Photodeposition system for micrometer-scale pattern fabrication. (B) Schematic of how the mask image is transmitted through the imaging fiber. The mask is reduced 15 times (93%) by the objective, thereby allowing large masks to be used for photopatterning. CCD camera, charge-coupled device camera.

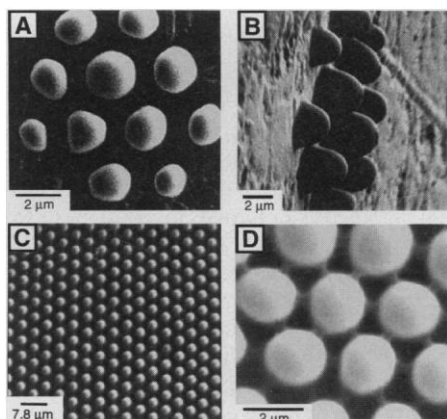
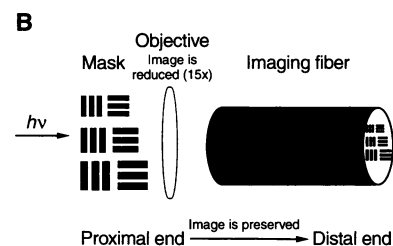
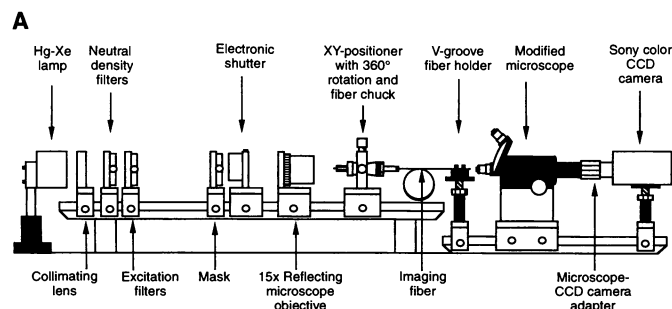


Fig. 2. (A) Scanning electron micrograph (SEM) of a photodeposited polydimethylsiloxane microstructure, fabricated with a pinhole mask, showing the hexagonal packing produced when optical imaging fibers are used as the microstructure substrate. (B) Side view SEM of the microstructure in (A) showing the polymer spot heights. (C) SEM of a monodisperse polymer array deposited on a defect-free imaging fiber. (D) SEM of a polymer microstructure with triangular-shaped wells between the polymer spots.

= 10^{-18} liters) and could potentially be used as miniature reaction vessels.

Polymer arrays were also produced with a standard air force resolution target (chrome on glass, Fig. 3A) as the photopatterning mask (Fig. 3B). It is important to note that the masks have dimensions 15 times as large as those of the desired microstructures, thereby facilitating the fabrication of complex micrometer-scale structures by relaxing the need to produce microscale masks.

We also deposited polymer arrays on substrates other than imaging fibers using a modification of the procedure described above. For example, a glass substrate was first functionalized with 3-trimethoxysilylpropylmethacrylate to facilitate polymer adhesion, and then 50 μl of polymerization solution (13) was pipetted onto the substrate. A nonfunctionalized imaging fiber was brought into contact with the substrate and positioned close to the glass surface, thus trapping a thin layer of polymerization solution. The solution was irradiated through the fiber for a fixed time

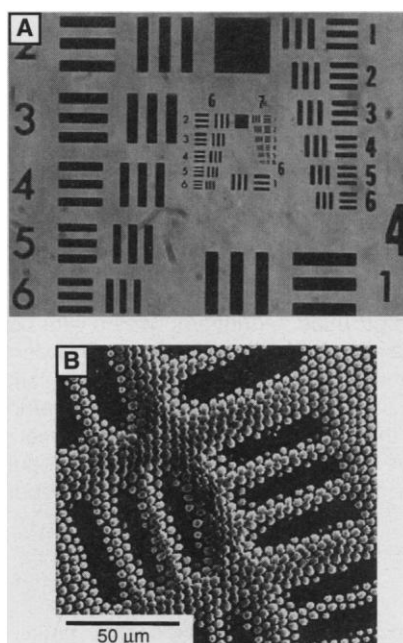


Fig. 3. (A) Light micrograph of a partial air force resolution target. The image was taken through a $10\times$ objective, so only the middle two groups could be observed. (B) SEM of a polymer microstructure produced with (A) as the mask. The groups of lines from top to bottom were produced from lines that were 176.7, 157.7, and 140.4 μm wide, respectively.

(14), and the fiber was then backed off and the substrate rinsed. Polymer deposition occurs on the substrate in a pattern corresponding to that of the optical fibers of the bundle. The SEM in Fig. 4 shows an array produced on a glass substrate. The monodisperse polymer spots have a diameter of 2.0 μm , a height of 0.3 μm , and are spaced 4.0 μm apart (15).

We have demonstrated the ability to fabricate micrometer-size polymer structures. These structures can be fabricated directly on optical imaging fibers as well as on other glass substrates, and the micrometer-size photopatterns are deposited with large, easily produced masks. The arrays of polymer spots can be monodisperse and highly ordered. The approach is general for any photopolymerizable monomer or oligomer; we have fabricated both

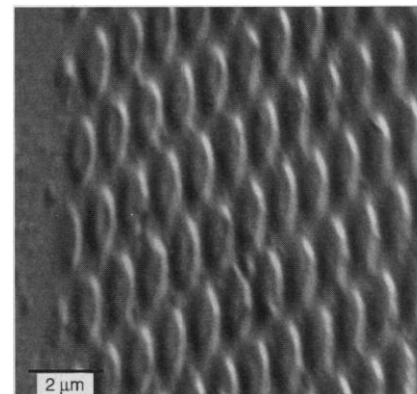


Fig. 4. SEM of a polymer microstructure deposited on a glass substrate.

hydrophilic and hydrophobic arrays with *N*-vinyl pyrrolidone and a photopolymerizable polydimethylsiloxane, respectively. By decreasing the monomer or oligomer concentration, the polymerization time, or both, polymer spots smaller than 2.5 μm , but with the same center-to-center spacing, can be produced. Polymer arrays with decreased polymer spacings could also be produced by using imaging fibers with smaller core diameters. Such arrays could have many uses because of their ease of fabrication, the diversity of polymer functionality, and their three-dimensional character. This last feature allows for high loadings of immobilized molecules, which we achieved by immobilizing fluorescent indicators in the polymer array for use as optical sensors (16). This polymeric microstructure array has the advantage that each polymer spot is not in contact with any other spots. Furthermore, each polymer spot of the array is connected to its own optical channel, allowing individual spots to be addressed with little or no crosstalk between adjacent spots.

REFERENCES AND NOTES

1. R. V. Parthasarathy and C. R. Martin, *Chem. Mater.* **6**, 1627 (1994); *Nature* **369**, 298 (1994); C. R. Martin, *Science* **266**, 1961 (1994).
2. T. Bein and C. Wu, *Chem. Mater.* **6**, 1109 (1994); T. M. Whitney, J. S. Jiang, P. C. Searson, C. L. Chien, *Science* **261**, 1316 (1993); J. D. Klein *et al.*, *Chem. Mater.* **5**, 902 (1993).
3. H. Noglik and W. J. Pietro, *Chem. Mater.* **6**, 1593

- (1994); H. S. Zhou, H. Sasahara, I. Honma, H. Komiyama, *ibid.*, p. 1534; B. O. Dabbousi, C. B. Murray, M. F. Rubner, M. G. Bawendi, *ibid.*, p. 216.
4. L. Shieh, Y. Tamada, A. Domb, R. Langer, *J. Controlled Release* **29**, 73 (1994); R. Gref *et al.*, *Science* **263**, 1600 (1994); R. Langer, *Acc. Chem. Res.* **26**, 537 (1993).
 5. M. Granström, M. Berggren, O. Inganäs, *Science* **267**, 1479 (1995).
 6. F. T. Wallenberger, *ibid.*, p. 1274 (1995).
 7. C. B. Gorman, H. A. Biebuyck, G. M. Whitesides, *Chem. Mater.* **7**, 252 (1995); R. Singhvi *et al.*, *Science* **264**, 696 (1994).
 8. C. Liu, H. Pan, M. A. Fox, A. J. Bard, *Science* **261**, 897 (1993).
 9. D. Noble, *Anal. Chem.* **67**, 201A (1995); S. P. A. Fodor *et al.*, *Science* **251**, 767 (1991).
 10. M. Yan, S. X. Cai, M. N. Wybourne, J. F. Keana, *J. Am. Chem. Soc.* **115**, 814 (1993); L. F. Rozsnyai, D.

- R. Benson, S. P. A. Fodor, P. G. Schultz, *Angew. Chem. Int. Ed. Engl.* **31**, 759 (1992).
11. Y. Chigusa, K. Fujiwara, Y. Hattori, Y. Matsuda, *Optoelectronics* **1**, 203 (1986); M. Mogi and K. Yoshimura, *Proc. Photo-Opt. Instrum. Eng.-Int. Soc. Opt. Eng.* **1067**, 172 (1989).
12. K. S. Bronk and D. R. Walt, *Anal. Chem.* **66**, 3519 (1994); S. M. Barnard and D. R. Walt, *Nature* **353**, 338 (1991).
13. A typical hydrophobic polymerization solution contained 500 μ l (15 to 20% acryloxypropyl-methylsiloxane) (80 to 85% dimethylsiloxane) copolymer (Gelest, Tullytown, PA), 30 mg of benzoin ethyl ether (Aldrich), and 1000 μ l of dichloromethane (Fisher). A typical hydrophilic polymerization solution contained 1 ml (5% ethylene glycol dimethacrylate, 95% *N*-vinyl pyrrolidone) of monomer (Aldrich), 60 mg of benzoin ethyl ether, and 1 ml of phosphate buffer (pH 7).

14. The light flux for deposition was 18.8 mW/cm², and the polymerization time was 1.5 s.
15. Measurements were obtained by atomic-force microscopy with a Digital Instruments Dimension 3000 scanning probe microscope. Microstructures on imaging fibers were analyzed in the tapping mode, whereas the microstructure on the glass substrate was analyzed in the contact mode.
16. B. G. Healy and D. R. Walt, unpublished results.
17. We gratefully acknowledge NIH (grant GM 48142) and the U.S. Department of Energy for financial support. The authors also would like to thank F. P. Milanovich, J. Richards, and S. Brown of Lawrence Livermore National Laboratories for their help in the design and fabrication of the polymer deposition system and Galileo Electro-Optics Corporation for the gift of imaging fiber.

28 March 1995; accepted 19 June 1995

Self-Condensing Vinyl Polymerization: An Approach to Dendritic Materials

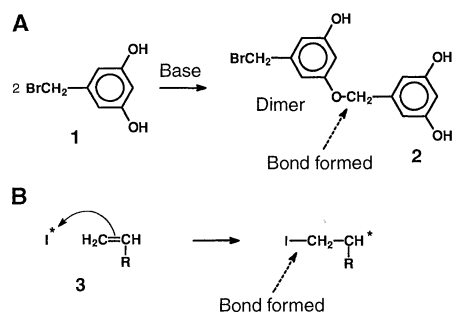
Jean M. J. Fréchet,* Masahiro Henmi, Ivan Gitsov, Sadahito Aoshima, Marc R. Leduc, R. Bernard Grubbs

Self-condensing vinyl polymerization was used to produce dendritic polymers with both highly branched structures and numerous reactive groups. A vinyl monomer will undergo self-polymerization if it contains a pendant group that can be transformed into an initiating moiety by the action of an external stimulus. The self-polymerization combines features of a classical vinyl polymerization process with those of a polycondensation because growth is accomplished by the coupling of reactive oligomers. Highly branched, irregular dendritic structures with a multiplicity of reactive functionalities are obtained by polymerization of 3-(1-chloroethyl)-ethenylbenzene.

The polymerization of vinyl monomers remains one of the most heavily used organic processes, and millions of tons of polymers are produced by this route every year. Despite increased sophistication in the design of catalysts, and the ability to better regulate growth processes, sequences of monomers, or the chain ends of polymers, "linear" propagation is the usual method of producing a relatively limited array of polymer architectures. The development of new polymer architectures is an important target because it is soon followed by findings of new properties and applications (1). For example, the globular shape of three-dimensional polymers such as dendrimers makes them attractive in applications ranging from catalysis to drug delivery systems. However, regular dendrimers are accessible only through multistep syntheses that limit their availability (1, 2). Less regular, hyperbranched polymers are more accessible, but their preparation has been restricted to the polycondensation of AB₂ monomers (3–5).

We now report a versatile approach to the production of highly branched polymer architectures in which a type of vinyl poly-

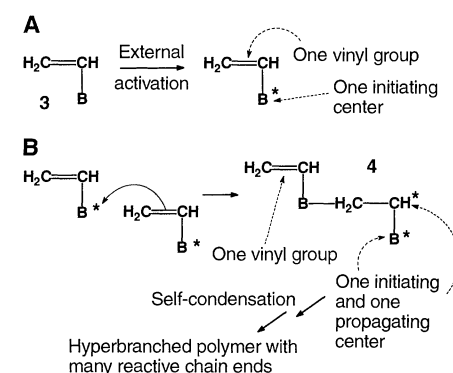
merization is encountered that proceeds with features normally associated with polycondensation reactions. The fundamental premise of our approach, in which an AB vinyl monomer is used to prepare a highly branched polymer, is contrasted with that in which an AB₂ monomer such as **1** is used to produce a hyperbranched polyether (Schemes 1 and 2). Williamson etherification of the benzylic bromide group A of **1** with one of the phenolic groups B of another monomer unit yields the dimer **2** (Scheme 1). The overall growth process involves two monomers containing a total



Scheme 1. (A) Typical polycondensation process. Addition does not create any new reactive centers. (B) Typical vinyl polymerization process. Addition creates a new reactive center.

of six potential reactive centers (2A + 4B) and gives rise to a dimer with only four remaining reactive centers (1A + 3B). Therefore, bond formation consumes two reactive centers (one A and one B), whereas the newly formed ether bond is incapable of participation in any further growth process. In the case of the AB vinyl monomer **3**, in which A is a vinyl group and B is a pendant group (for example, the aromatic ring of styrene), the polymerization is started by an activated initiating moiety, I*. Depending on the type of polymerization, I* could be a "living" free radical, an electrophilic cationic moiety, or a carbanion. In addition, reaction of I* with one carbon atom of the double bond (DB) results in the consumption of two reactive centers with concurrent formation of a bond that is usually incapable of further reaction. However, the process also creates a new active site on the second carbon atom of the DB (Scheme 1) that is capable of reacting with yet another DB in the process of propagation. Because the DB behaves as an effective difunctional moiety, the foundation may be laid for growth of highly branched structures through appropriate manipulations of the pendant group B.

Scheme 2 outlines the basic concept of self-condensing vinyl polymerization. The AB vinyl monomer **3** is now selected with a



Scheme 2.

Baker Laboratory, Department of Chemistry, Cornell University, Ithaca, NY 14853-1301, USA.

*To whom correspondence should be addressed.